Author(s): Li, Z.

Title: Accuracy analysis of a mesh refinement method using benchmarks of 2-D lid-driven cavity flows and finer meshes

Journal: Journal of Mathematical Chemistry

ISSN: 0259-9791 **Year:** 2014 **Pages:** 1156 - 1170

Volume: 52 **Issue:** 4

Abstract: Lid-driven cavity flows have been widely investigated and accurate results have been achieved as benchmarks for testing the accuracy of computational methods. This paper verifies the accuracy of a mesh refinement method numerically using two-dimensional steady incompressible lid-driven flows and finer meshes. The accuracy is shown by comparing the coordinates of centres of vortices located by the mesh refinement method with the corresponding benchmark results. The accuracy verification shows tha ...

Noname manuscript No.
(will be inserted by the editor)

Accuracy analysis of a mesh refinement method using benchmarks of 2-D lid-driven cavity flows and finer meshes

Zhenquan Li

Received: date / Accepted: date

Abstract Lid-driven cavity flows have been widely investigated and accurate results have been achieved as benchmarks for testing the accuracy of computational methods. This paper verifies the accuracy of a mesh refinement method numerically using two-dimensional steady incompressible lid-driven flows and finer meshes. The accuracy is shown by comparing the coordinates of centres of vortices located by the mesh refinement method with the corresponding benchmark results. The accuracy verification shows that the mesh refinement method provides refined meshes that all centres of vortices are contained in refined grids based on the numerical solutions of Navier-Stokes equations solved by finite volume method except for one case. The well known SIMPLE algorithm is employed for pressure-velocity coupling. The accuracy of the numerical solutions is shown by comparing the profiles of horizontal and vertical components of velocity fields with the corresponding components of the benchmarks and also streamlines. The mesh refinement method verified in this paper can be applied to find the accurate numerical solutions of any mathematical models containing continuity equations for incompressible fluid or steady state fluid flows or heat transfer.

Keywords Mesh refinement · Lid-driven cavity flow · finite volume method

1 Introduction

Meshing is the process of breaking up a physical domain into smaller subdomains (called elements or cells or grids) in order to evaluate the numerical

Z. Li
School of Computing and Mathematics, Charles Sturt University, Thurgoon, New South Wales 2640, Australia.
Tel.: +61-265019604
Fax: +61-260519604
E-mail: jali@csu.edu.au

solutions of differential equations. Adaptive mesh refinement is a computational technique to improve the accuracy of numerical solutions of differential equations by starting the calculations on a coarse basic mesh (initial mesh) and then refining this mesh where less accuracy may occur locally.

There are a large number of publications on adaptive mesh refinements and their applications. Some of adaptive refinement methods use a refinement criterion which is based on local truncation errors (e.g. Almgren, Bell, Colella, Howell & Welcome [1]; Bell, Berger, Saltzman & Welcome [3]; Berger & Oliger [4]; Berger & Colella [5]). Other common adaptive mesh refinement methods include h-refinement(e.g. Lohner [22]; Speares & Berzins [25]), p-refinement (e.g. Bell, Berger, Saltzman & Welcome [3]; Zienkiewicz, Kelly & Gago [27]) or r-refinement (e.g. Miller & Miller [23]; Mosher [24]), with different combinations of these also possible (e.g. Capon & Jimack [6]; Demkowicz, Oden, Rachwicz & Hardy [7]). The overall aim of these adaptive algorithms is to allow a balance to be obtained between accuracy and computational efficiency. The h-refinement is a method where meshes are refined and/or coarsened to achieve a prescribed accuracy and efficiency. The p-refinement is a method where the accuracy orders are assigned to grids to achieve exponential convergence rates and r-refinement is a method where grids are moved and redistributed to track evolving non-uniformities. In summary, all these mesh refinement methods are proposed based on the quantitative considerations of numerical solutions of differential equations.

We proposed adaptive mesh refinement methods from a different point of view for 2-D velocity fields (Li [16]) and for 3-D velocity fields (Li [15]) based on a theorem in qualitative theory of differential equations (Theorem 1.14, page 18, Ye et al. [26]). The theorem indicates that a divergence free vector field has no limit cycles or one sided limit cycles, that is, the trajectories (or streamlines) of divergence free vector fields are closed curves in bounded domains (singular points are streamlines). The adaptive mesh refinement methods adaptively refine the mesh based on the information of numerical velocity fields evaluated on it. Using numerical velocity fields obtained by taking the vectors of the analytical velocity fields at nodes of meshes, examples showing the accuracy of the methods include: locating the singular points and asymptotic lines for two-dimensions [16]; the singular points and asymptotic plane for three-dimensions [15]; and drawing closed streamlines (Li [13], [14]) using the refined meshes with a pre-specified number of refinements of the initial meshes. We have verified that the accuracies of the proposed adaptive mesh refinement method in identifying asymptotic line for T from 1 to 5, and identifying singular points and drawing closed streamlines for T from 1 to 4 by two analytical velocity field examples [16]. We have also verified that the larger the value of T, the more accurate are the location of the asymptotic line, the coordinates of the singular points and the closed streamline [16]. Identification of accurate locations of singular points and asymptotic lines (planes), and drawing closed streamlines are some of the accuracy measures for computational methods.

We showed that the adaptive mesh refinement method for 2-D velocity fields provides accurate estimates for the singular points of 2-D steady in-

compressible lid-driven cavity flows using the numerical velocity fields (Li & Lal [20]). The numerical velocity fields are obtained by solving the Navier–Stokes equations with the boundary conditions numerically using a second order colocated finite volume method (GSFV) with a splitting method for time discretization (Faure, Laminie & Temam [9]). We applied the adaptive mesh refinement method to the initial meshes and the numerical velocity fields, and take the centres of refined grids in the vortex regions as the estimates of the singular points. The comparison of the estimates with the benchmarks shows that the estimates for the singular points are accurate.

The accuracy of the mesh refinement method using two-dimensional lid-driven cavity flow and a different finite volume method has been established using coarser meshes (65×65 for Re = 1000 and 85×85 for Re = 2500) [21]. It shows that mesh refinement is necessary if we want the relative error of the centre coordinates of tertiary vortices less than 40%. This paper investigates whether mesh refinement is needed for finer initial meshes.

2 Algorithm of mesh refinement and finite volume method

In this section, we summarize the adaptive mesh refinement method based on the continuity equation (Li [16]) and the finite volume method used (Ferziger & Peric [10]).

Assume that $\mathbf{V}_l = \mathbf{A}\mathbf{X} + \mathbf{B}$ is a vector field obtained by linearly interpolating the vectors at the three vertexes of a triangle, where

$$\mathbf{A} = \begin{pmatrix} a_{11} & a_{12} \\ a_{21} & a_{22} \end{pmatrix}, \quad \mathbf{B} = \begin{pmatrix} b_1' \\ b_2' \end{pmatrix}$$

are constant matrices and vertical vector respectively, and $\mathbf{X} = (x_1, x_2)^T$. $\mathbf{V}_l$ is unique if the area of the triangle is not zero [17]. Mass conservation for an incompressible fluid means that

$$\nabla \cdot \mathbf{V}_l = \mathrm{trace}(\mathbf{A}) = 0. \tag{1}$$

Let f be a scalar function depending only on spatial variables. We assume that $f\mathbf{V}_l$ satisfies equation (1) and then calculate the expressions of f. Li [16] gives the expressions of f for the four different Jacobian forms of coefficient matrix $\mathbf{A}$ in Table 1. The conditions (MC)(MC is the abbreviation of mass conservation) are the functions f in Table 1 not equaling zero or infinity at any point on the triangular domains when $f\mathbf{V}_l$ satisfies Equation (1) on these triangular domains.

We review the algorithm of adaptive mesh refinement for quadrilateral mesh used in this paper. The algorithm is also applicable to triangular meshes. The following grid refinement algorithm describes how to use the conditions (MC) to refine a quadrilateral grid in a given mesh. To avoid an infinite refinement of the mesh, we choose a pre-specified threshold number of refinements T based on the accuracy requirements. The algorithm of grid refinement is:

Step 1 Subdivide a quadrilateral grid into two triangles, obtain $\mathbf{V}_l$ by linearly interpolating the given numerical velocity field and check if $\mathbf{V}_l$ satisfies Equation (1) on both triangles. If yes, there is no refinement for the quadrilateral grid. If no, go to Step 2.

Step 2 Apply the conditions (MC) to both of the triangles. If the conditions (MC) are satisfied on both triangles, there is no refinement for the quadrilateral grid. Otherwise, we subdivide the grid into a number of small grids such that the lengths of all sides of the small grids are truly reduced (e.g. connecting the mid-points of opposite sides of a quadrilateral by line segments produces four small quadrilaterals and the lengths of the sides of the four small quadrilaterals are truly reduced).

The algorithm of adaptive mesh refinement is:

Step 1 Evaluate the numerical velocity field for a given initial mesh;

Step 2 Refine the grids of the mesh one by one using the above grid refinement algorithm;

Step 3 Take the refined mesh as initial mesh and go to Step 1 until a satisfactory numerical velocity field is obtained or the threshold number T is reached.

In Section 3, we use the finite volume method with SIMPLE algorithm for pressure-velocity coupling to evaluate numerical velocity fields [10]. This finite volume method has different arrangement for pressure-velocity from the finite volume method we used before [9].

In this paper, we subdivide a quadrilateral by connecting the mid-points of the two opposite sides of a quadrilateral and the threshold number T=1, i.e., we subdivide a cell once only for testing the accuracy of the refinement method.

3 Accuracy analysis by comparisons with benchmarks

We take the results obtained by using a mesh with 601×601 uniform grids, stream function and vorticity as the benchmarks (Erturk *et al.* [8]). We consider the accuracy of the mesh refinement method in the following two aspects:

- the variations of the refined meshes according to the comparison of horizontal and vertical profiles of the numerical velocity fields with the corresponding benchmarks.
- inclusion of the centres of vortices located in the benchmarks in the refined mesh.

3.1 Variation of refined meshes

We consider the refined meshes for two-dimensional lid-driven cavity flows for different mesh sizes and Reynolds number Re = 1000, 2500, and 5000, respectively. We show horizontal profiles at $x = 0.5$ and vertical velocity profiles at

$y = 0.5$ as the corresponding benchmarks are known, streamlines of $\mathbf{V}_l$, and refined meshes. The streamlines are generated by *Matlab* function streamline. A grid is said to be a refined grid if a cross is drawn inside.

One of the possible comparisons is the adaptive mesh refinement which refines everywhere that solution gradients are large (Henderson [11], 293-299). The refinement criteria enforce

$$\| \nabla u^{(k)} \| \leq \epsilon \| u^h \|_1$$

everywhere in the mesh, where $\| \cdot \|$ is the L_2 norm, $\| \cdot \|_1$ is the H^1 norm, ϵ is the discretization tolerance, u^h is finite-dimensional approximation for u, and k in $\| \nabla u^{(k)} \|$ is the number of subdomains. Figure 5.7 of [11] shows the refined meshes for $\epsilon = 10^{-3}$, 10^{-4}, 10^{-5}, and 10^{-6} for lid-driven cavity flow at Re = 1000. Even though there might be some relations between the refined meshes and the vorticity field as ϵ decreases, no one provides any information on the pattern of the flow field such as locations of the centres of vortices and separation curves of the regions (e.g., primary and secondary vortex regions).

3.1.1 Re = 1000

We show the figures for Re = 1000 generated from a mesh with 99×99 uniform grids. From Figure 1, the horizontal profile u of the numerical velocity field at $x = 0.5$ shows a slight difference with the corresponding benchmark. From Figure 2, the vertical profile v of the numerical velocity field at $y = 0.5$ fits the benchmark well. However, the horizontal and vertical profiles reflect the local accuracy of the numerical velocity field. The streamlines in Figure 3 provide the global accuracy of the numerical velocity field depending on the accuracy of streamline generation method. The streamlines in Figure 3 are not closed (spiral lines) so we conclude that the velocity field $\mathbf{V}_l$ does not satisfy Equation (1) [26,8] or f does not satisfy the condition (MC) on some grids in the regions. Figure 4 shows the refined mesh. There are three isolated grids in the refined mesh: one in the primary region and two in the secondary regions. The refined grid in the primary regions contains the centre of primary vortex, and the isolated refined grid on the bottom left side contains the centre of the bottom left secondary vortex, and the isolated refined grid on the bottom right side contains the centre of the bottom right secondary vortex (refer to Table 1). Even though the centres of tertiary vortices are included in the refined grids, we can not identify the grids in the refined mesh. Further mesh refinement is needed for more information on this matter.

3.1.2 Re = 2500

We show the figures for Re = 2500 generated from a mesh with 121×121 uniform grids. From Figure 5, the difference between the horizontal profile u of the numerical velocity field at $x = 0.5$ and the corresponding benchmark is small. From Figure 6, the vertical profile v of the numerical velocity field

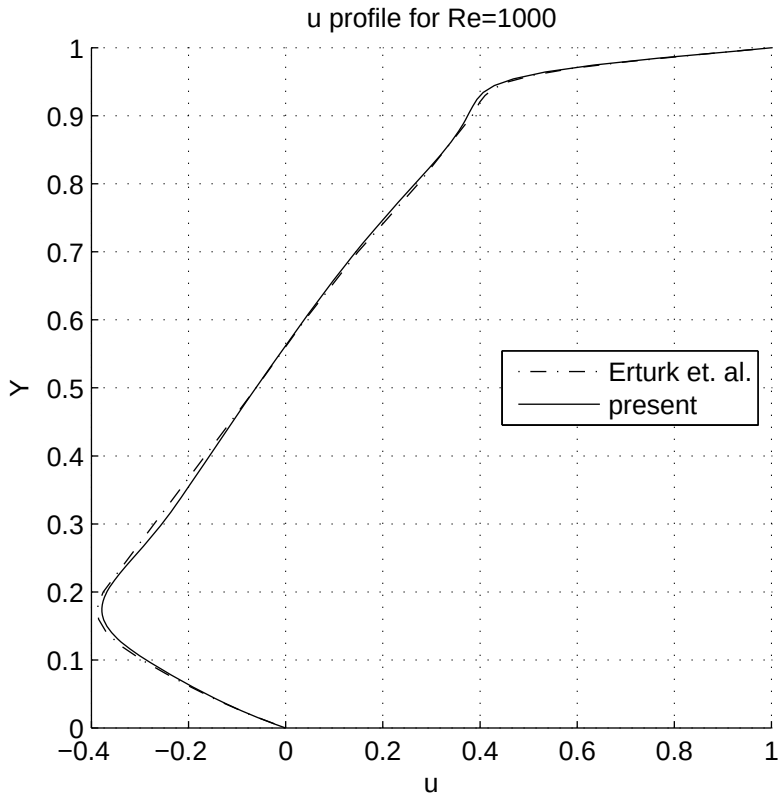

Fig. 1 Horizontal profile of velocity field at $x = 0.5$ for mesh size 99×99.

at $y = 0.5$ fits the corresponding benchmark well. The streamlines in the primary vortex region in Figure 7 are almost closed with very small errors. If the errors come from the process of generating of streamline, we conclude that the velocity field $\mathbf{V}_l$ satisfies Equation (1) or f satisfies the condition (MC) and there is no refinement in the region. If the errors come from the numerical velocity field, there are refinements in the region. There is no refinement in the primary vortex region in Figure 8 so the errors shown in Figure 7 come from the generation of the streamlines. The difference between the coordinates of the centre of primary vortex from the benchmark and linearly interpolated velocity field $\mathbf{V}_l$ is shown in Table 1. Even though the centre of primary vortex is not shown in Figure 8 due to the accuracy of the linearly interpolated velocity field in the primary region, the centre of an extra tertiary vortex is shown in the bottom right corner. The three isolated refined grids in the two bottom corners include the centres of two secondary and one tertiary vortices (refer to Table 1).

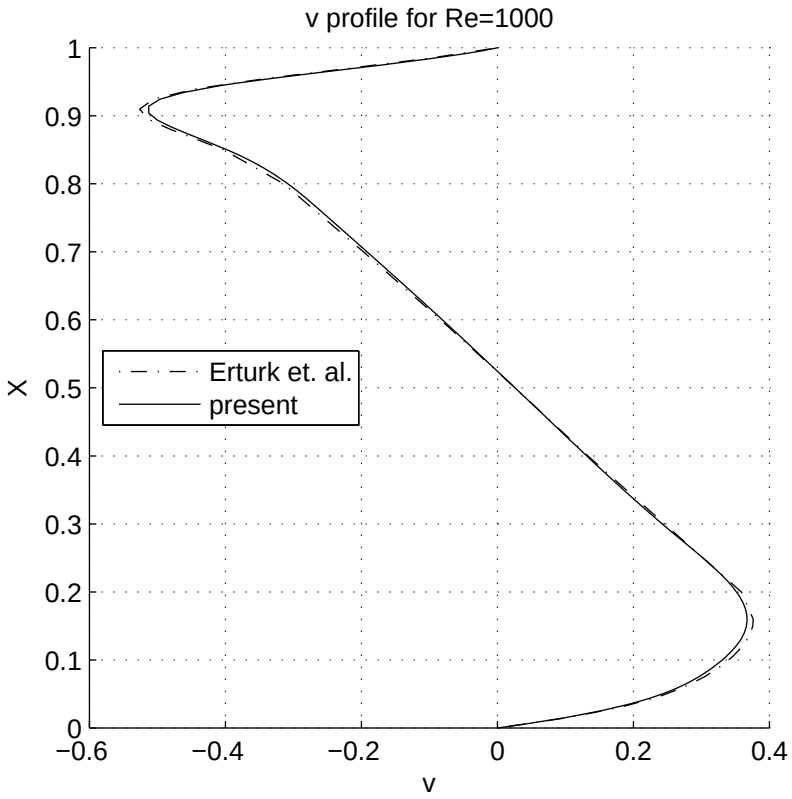

Fig. 2 Vertical profile of velocity field at $y = 0.5$ for mesh size 99×99.

3.1.3 Re = 5000

This section shows the figures for Re = 5000 generated from a mesh with 139×139 uniform grids and the analysis. Figure 9 shows the difference between the horizontal profile u of the numerical velocity field at $x = 0.5$ and the corresponding benchmark. The difference is not small. From Figure 10, the difference between the vertical profile v of the numerical velocity field at $y = 0.5$ and the corresponding benchmark is similar to that of the profile of u. The streamlines in the primary vortex region in Figure 11 are also almost closed with very small errors. Combining the horizontal and vertical profiles of the velocity field with the streamlines in the primary vortex region, we conclude that the numerical velocity filed is not accuracy enough for a reasonable accuracy requirement. The accuracy can be improved by increasing the mesh size. Figure 12 confirms the conclusion. As the same case as Re = 1000, there is a refined cell in the primary vortex region in Figure 12. However, the refined mesh shows more complicated structure in the corners. The isolated refined grid in the primary region contains the centre of primary vortex. The three

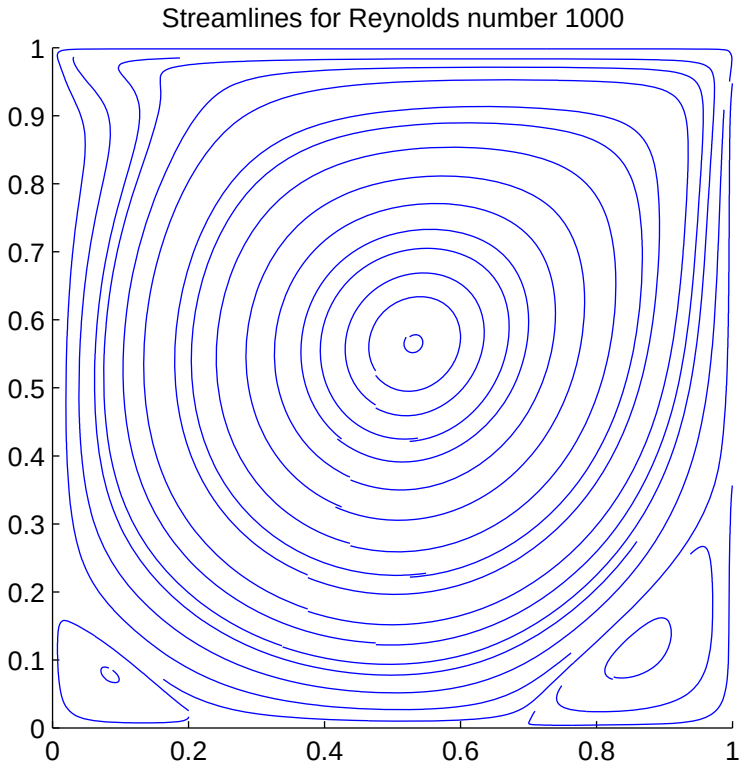

Fig. 3 Streamlines for mesh size 99×99.

isolated refined grids in the two bottom corners include the centres of two secondary and one tertiary vortices (refer to Table 1).

3.1.4 Vortex centre locations

This subsection shows the comparison of the centres of vortices between the benchmarks and the corresponding estimates obtained in this paper.

Table 1 presents that coordinates of centres of vortices in the benchmark (blue) and the corresponding coordinates for Re = 1000, 2500, and 5000 from the linearly interpolated velocity fields $\mathbf{V}_l$. In this table, the abbreviations BR, BL and TL refer to bottom right, bottom left and top left corners of the cavity, respectively. The numbers following these abbreviations refer to the vortices that appear in the flow, which are numbered according to size (e.g. BR1 refers to bottom right secondary vortex, and BR2 refers to bottom right tertiary vortex, etc.).

Even though the estimate for coordinates of the centre of primary vortex for Re = 5000 is more accurate than that for Re = 2500 because of the finer

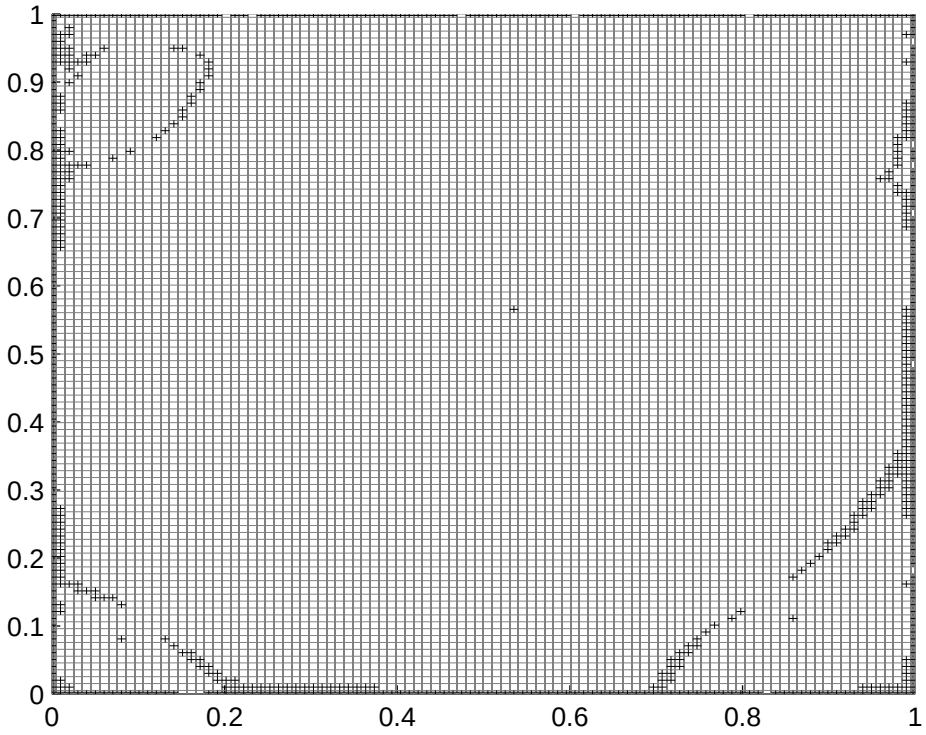

Fig. 4 Refined mesh for Re = 1000 with mesh size 99×99.

Table 1 Locations of the centre of vortices

Vortex type	Reynolds numbers		
	Re = 1000(99×99)	Re = 2500(121×121)	Re = 5000(139×139)
Primary vortex	(0.5316,0.5659) (0.5300,0.5650)	(0.5202,0.5446) (0.5200,0.5433)	(0.5155,0.5357) (0.5150,0.5350)
BR1	(0.8634,0.1128) (0.8633,0.1117)	(0.8318,0.0910) (0.8350,0.0917)	(0.8037,0.0729) (0.8050,0.0733)
BL1	(0.0839,0.0779) (0.0833,0.0783)	(0.0845,0.1108) (0.0850,0.1100)	(0.0731,0.1370) (0.0733,0.1367)
BR2	- (0.9917,0.0067)	(0.9851,0.0056) (0.9900,0.0100)	(0.9743,0.0201) (0.9783,0.0183)
BL2	(0.0075,0.0075)) (0.0050,0.0050)	(0.0090,0.0083) (0.0067,0.0067)	(0.0079,0.0099) (0.0083,0.0083)
TL1	- -	(0.0441,0.8904) (0.0433,0.8900)	(0.0641,0.9105) (0.0633,0.9100)
BR3	- -	- -	(0.9397,0.0043) (0.9983,0.0017)

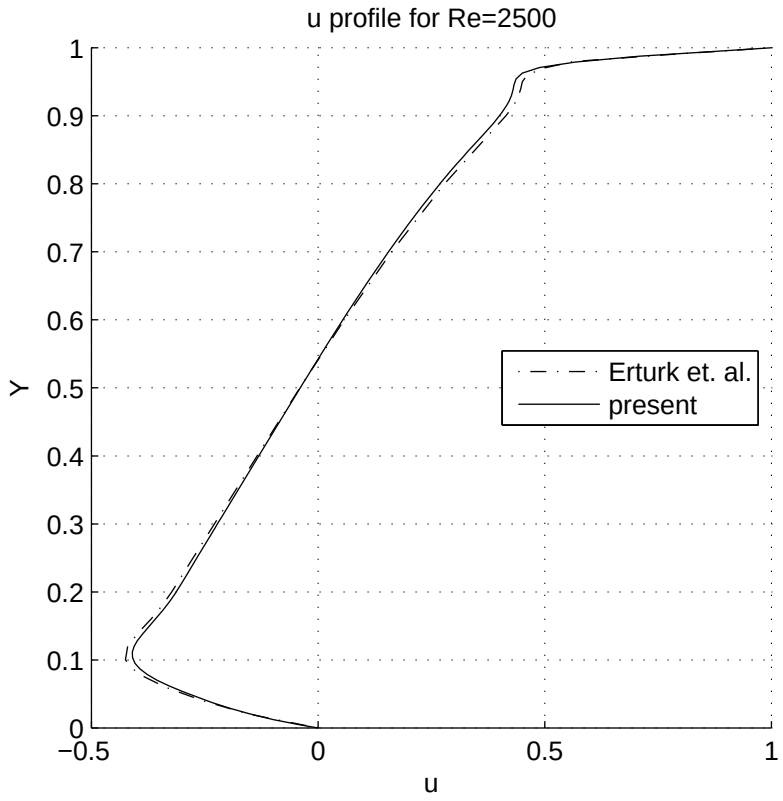

Fig. 5 Horizontal profile of velocity field at $x = 0.5$ for mesh size 121×121.

mesh, the streamlines in the primary vortex region for Re = 5000 in Figure 11 have larger error than those for Re = 2500 in Figure 7. The reason is that the coordinates of centres of the velocity fields are estimated by the coordinates of the centres of the linearly interpolated velocity fields $\mathbf{V}_l$. The coordinates of the centre of tertiary vortex in the bottom right corner for Re = 1000 is not listed in Table 1 and not shown in refined grids in Figure 4. Further refinement may find the centre as indicated in the examples of the analytical velocity fields [16]. Table 2 shows the relative errors of the estimated centre locations of vortices. Except for bottom left secondary vortices (BL2), all estimates are acceptable for relative error less than 1 %. Further refinement is needed to find more accurate estimate locations of bottom left secondary vortices.

3.2 Refined grids containing centres of vortices

We take Re = 2500 as an example to verify if the centres of vortices are contained in refined grids of refined mesh except the centre of the primary vortex.

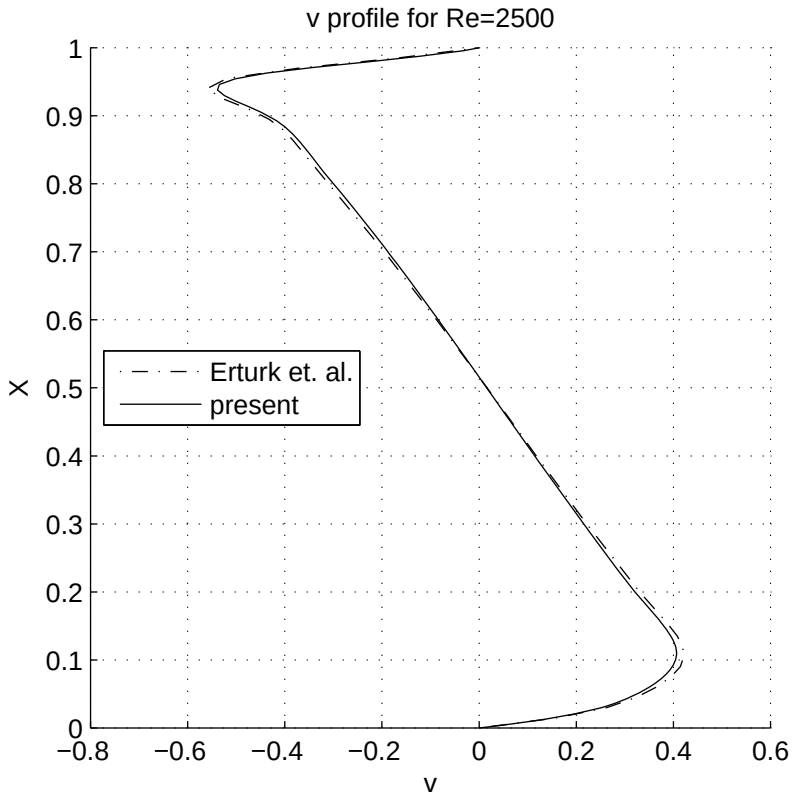

Fig. 6 Vertical profile of velocity field at $y = 0.5$ for mesh size 121×121.

Table 2 Relative errors of the estimates of vortex centres

Vortex type	Reynolds numbers		
	Re = 1000(99×99)	Re = 2500(121×121)	Re = 5000(139×139)
Primary vortex	0.0024	0.0017	0.0012
BR1	0.0013	0.0039	0.0017
BL1	0.0063	0.0068	0.0023
BR2	-	0.0067	0.0045
BL2	0.5000	0.2957	0.1405
TL1	-	0.0010	0.0010
BR3	-	-	0.0588

If the centres of vortices are included in refined grids, further refinements of the mesh will provide more accurate estimate locations of the centres. The following figures show the sub plots of bottom left, bottom right and top left corners of refined mesh for Re = 2500. The red dots are the centres given in the benchmark [8]. We conclude that the centres are contained in refined grids in these enlarged sub plots clearly. Figure 13 shows the refined mesh and the centres of vortices in region [0 0.3]×[0 0.3]. The centre of the secondary

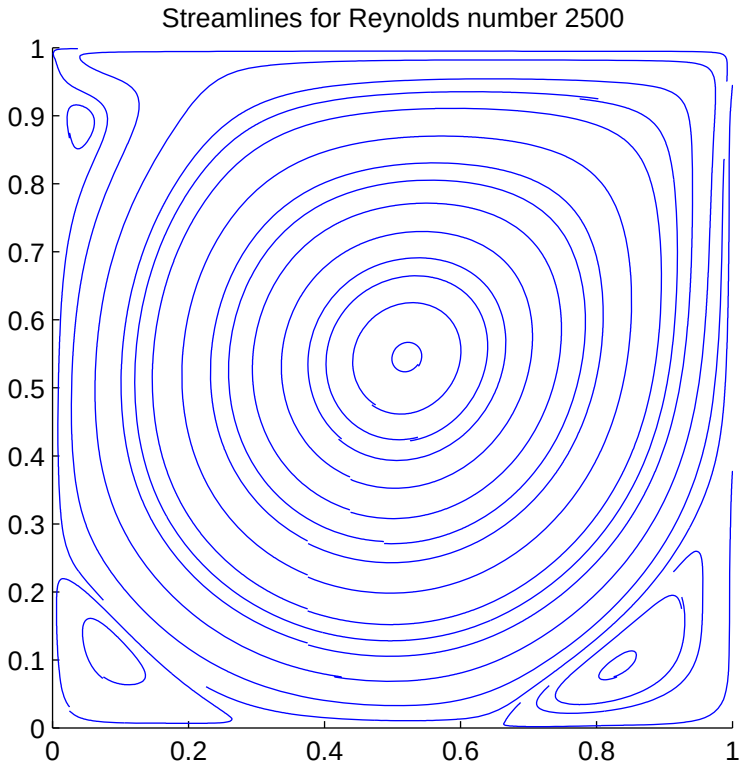

Fig. 7 Streamlines for mesh size 121×121.

vortex is not located at the centre of the refined grid. Figure 14 shows the refined mesh and the centres of vortices in region [0.6 1]×[0 0.4]. The centre of the secondary vortex is almost located at the centre of the refined grid. Figure 15 shows the refined mesh and the centre of the secondary vortex in region [0 0.3]×[0.7 1]. The centre of the secondary vortex is not located at the centre of refined grid.

4 Discussions

We considered the adaptive mesh refinement method using three cases for two dimensional lid-driven cavity flows. We use horizontal and vertical profiles of velocity fields at $x = 0.5$ and $y = 0.5$ respectively and the streamlines generated by *Matlab* for the accuracy of the numerical velocity fields. We then consider whether the refined meshes can locate the centres of vortices. Besides the centre of primary vortex for Re = 2500 which has been estimated accurately, the other centres of vortices locate in the refined grids in the refined

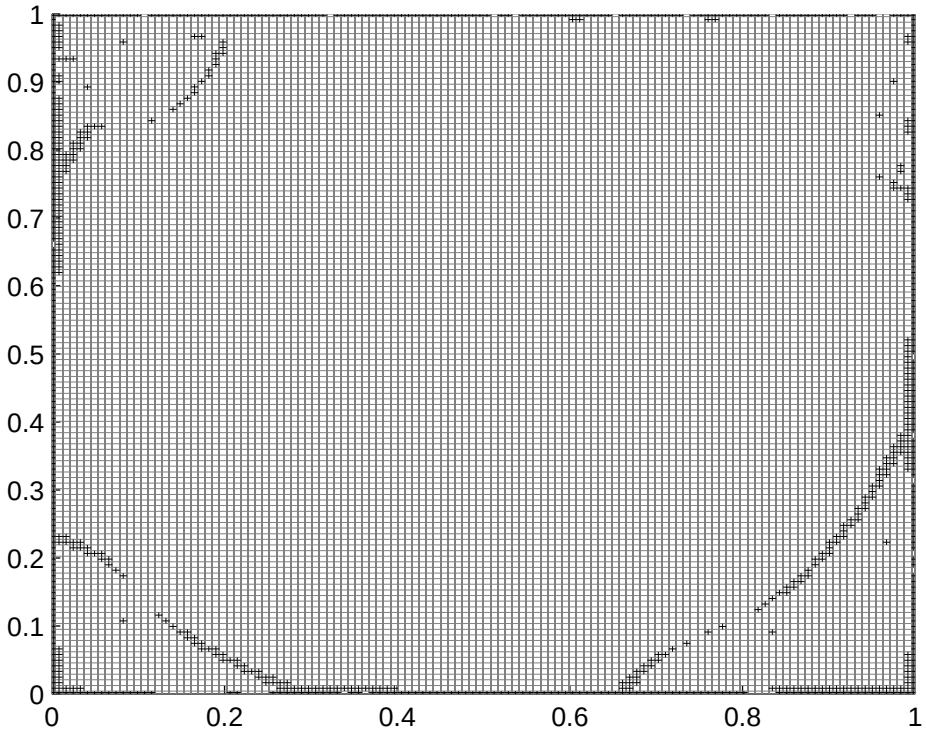

Fig. 8 Refined mesh for Re = 2500 with mesh size 121×121.

meshes. Further refinement is necessary if we need more accurate coordinates of centres of BL2 with smaller relative errors for these three cases.

References

1. A. S. Almgren, J. B. Bell, P. Colella, L. H. Howell and M. L. Welcome, A conservative adaptive projection method for the variable density incompressible Navier–Stokes equations, *J. of Computational Physics*, **142**, 1–46 (1998)
2. B. F. Armaly, F. Durst, J. C. F. Pereira and B. Schonung, Experimental and theoretical investigation of backward-facing step flow, *J. Fluid Mech.*, **127**, 473–496 (1983)
3. J. Bell, M. Berger, J. Saltzman and M. Welcome, Three-dimensional adaptive mesh refinement for hyperbolic conservation laws, *SIAM J. of Scientific Computing*, **15**, 127–138 (1994)
4. M. J. Berger and J. Oliger, Adaptive mesh refinement for hyperbolic partial differential equations, *J. of Computational Physics*, **53**, 484–512 (1984)
5. M. J. Berger and P. Colella, Local adaptive mesh refinement for shock hydrodynamics, *J. of Computational Physics*, **82**, 64–84 (1989)
6. P. J. Capon and P. K. Jimack, An adaptive finite element method for the compressible Navier–Stokes equations, In M. J. Baines and K. W. Morton, editors, *Numerical Methods for Fluid Dynamics*, 5. OUP (1995)

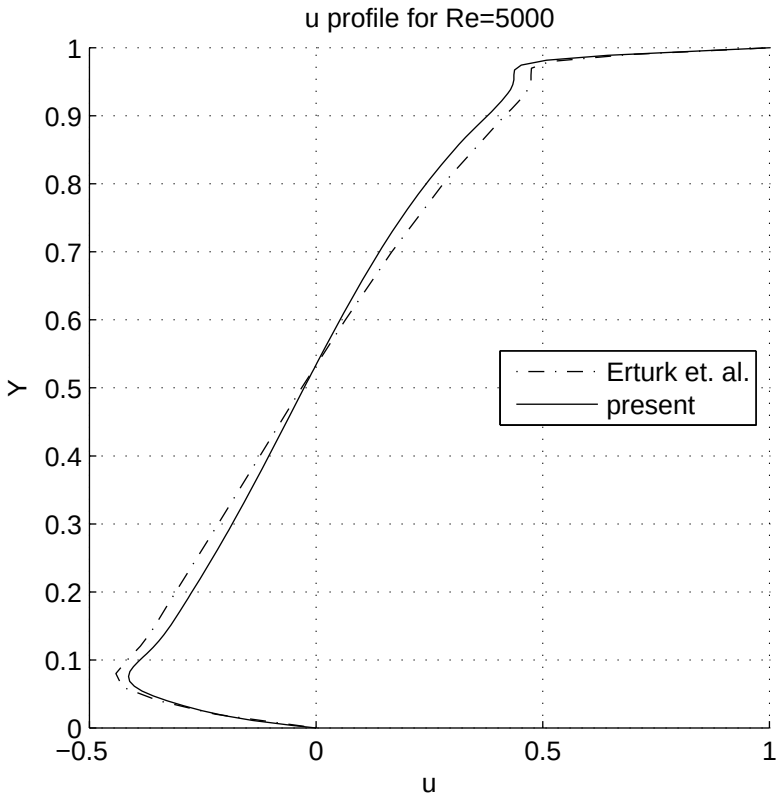

Fig. 9 Horizontal profile of velocity field at $x = 0.5$ for mesh size 139×139.

7. L. Demkowicz, J. T. Oden, W. Rachwicz and O. Hardy, An h-p Taylor–Galerkin finite element method for the compressible Euler equations, *Computer Methods in Applied Mechanics and Engineering*, **88**, 363–396 (1991)
8. E. Erturk, T. C. Corke and C. Gökcöl, Numerical solutions of 2-D steady incompressible driven cavity flow at high Reynolds numbers, *International Journal for Numerical Methods in Fluids*, **48**, 747–774 (2005)
9. S. Faure, J. Laminie and R. Temam, Colocated finite volume schemes for fluid flows, *Communication in Computational Physics*, **4**, 1–25 (2008)
10. J. H. Ferziger and M. Peric, *Computational methods for fluid dynamics*, Springer-Verlag, Berlin Heidelberg, 3ed (2002)
11. R. D. Henderson, Adaptive spectral element methods for turbulence and transition, In T. J. Barth and H. Deconinck, editors, *High-Order Methods for Computational Physics*, Springer-Verlag, Berlin Heidelberg (1999)
12. Z. Li, A mass conservative streamline tracking method for two dimensional CFD velocity fields, *J. of Flow Visualization and Image Processing*, **9**, 75–87 (2002)
13. Z. Li, An adaptive streamline tracking method for two-dimensional CFD velocity fields based on the law of mass conservation, *J. of Flow Visualization and Image Processing*, **13**, 1–14 (2006)
14. Z. Li, An adaptive streamline tracking method for three-dimensional CFD velocity fields based on the law of mass conservation, *J. of Flow Visualization and Image Processing*, **13**, 359–376 (2006)

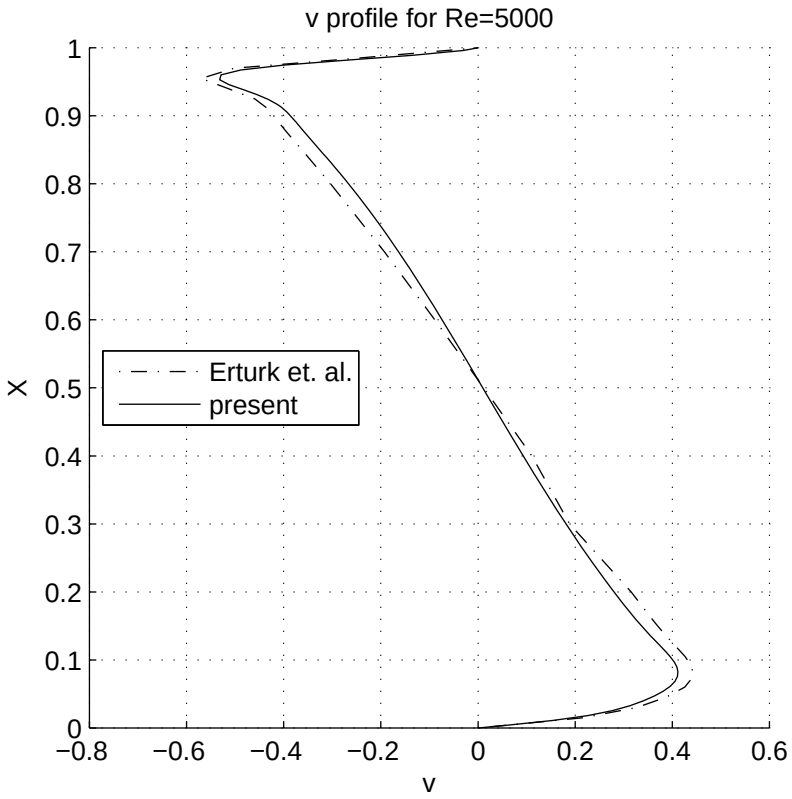

Fig. 10 Vertical profile of velocity field at $y = 0.5$ for mesh size 139×139.

15. Z. Li, An adaptive three-dimensional mesh refinement method based on the law of mass conservation, *J. of Flow Visualization and Image Processing*, **14**, 375–395 (2007)
16. Z. Li, An adaptive two-dimensional mesh refinement method based on the law of mass conservation, *J. of Flow Visualization and Image Processing*, **15**, 17–33 (2008)
17. Z. Li and G. Mallinson, Mass conservative fluid flow visualisation for CFD velocity fields, *KSME International Journal*, **15**, 1794–1800 (2001)
18. Z. Li and R. Lal, An application of a mesh refinement method based on the law of mass conservation, *Proceedings of 2010 International conference on Computational and Infomraiton Sciences*, 226–229. IEEE CPS (2010)
19. Z. Li, An application of a mesh refinement to lid-driven cavity flow, *Proceedings of FLUCOME 2011*, paper no. 241
20. Z. Li and R. Lal, Sensitivity analysis of a mesh refinement method using the numerical solutions of 2-D steady incompressible driven cavity flow, *submitted for publication*
21. Z. Li, Accuracy analysis of an adaptive mesh refinement method using benchmarks of 2-D steady incompressible lid-driven cavity flows, *submitted for publication*
22. R. Lohner, An adaptive finite element scheme for transient problems in CFD, *Computer Methods in Applied Mechanics and Engineering*, **61**, 323–338 (1987)
23. K. Miller and R. Miller, Moving finite elements, Part I, *SIAM Journal on Numerical Analysis*, **18**, 1019–1032 (1981)
24. M. C. Mosher, A variable node finite element method, *J. of Computational Physics*, **57**, 157–187 (1985)

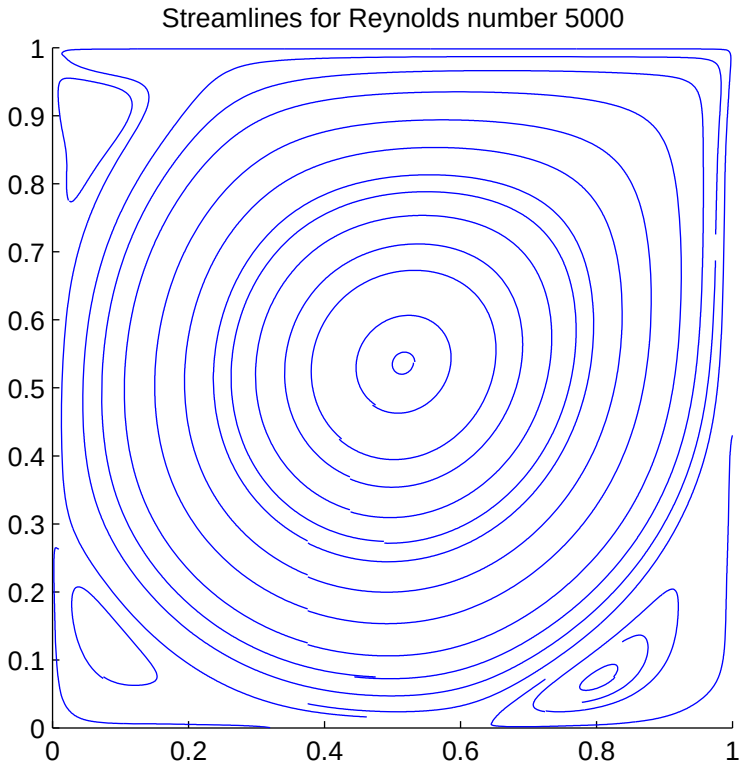

Fig. 11 Streamlines for mesh size 139×139.

25. W. Speares and M. Berzins, A 3-D unstructured mesh adaptation algorithm for time-dependent shock dominated problems, *International Journal for Numerical Methods in Fluids*, **25**, 81–104 (1997)
26. Y. Ye and Others, *Theory of limit cycles*, American Mathematical Society Press (1986)
27. O. C. Zienkiewicz, D. W. Kelly and J. P. Gago, The hierarchical concept in finite element analysis, *Computer & Structures*, **16**, 53–65 (1983)

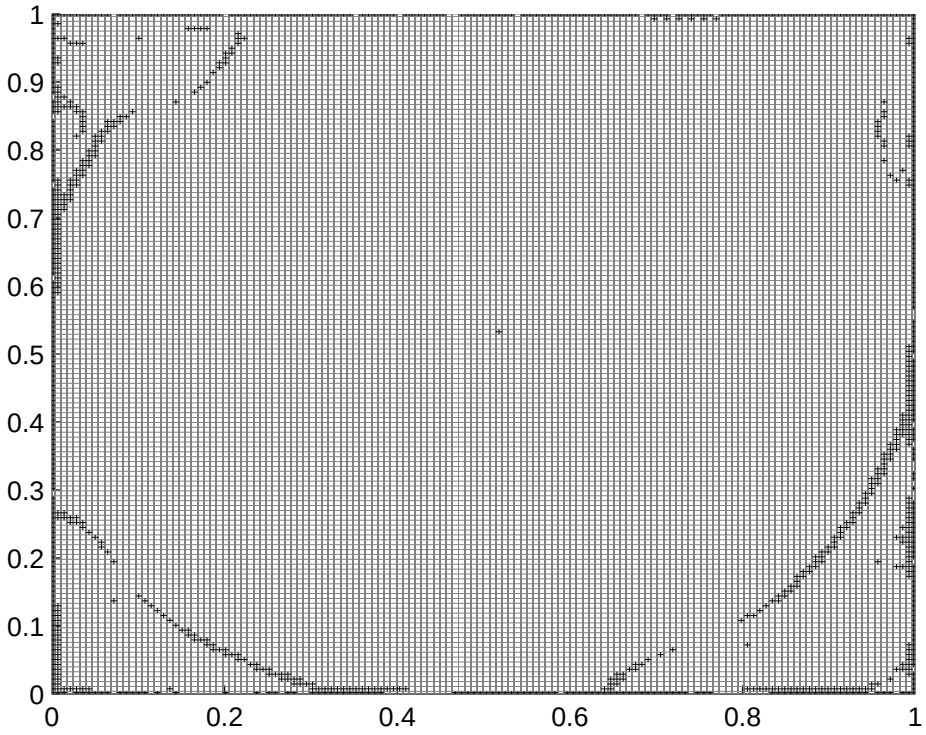

Fig. 12 Refined mesh for Re = 5000 with mesh size 139×139.

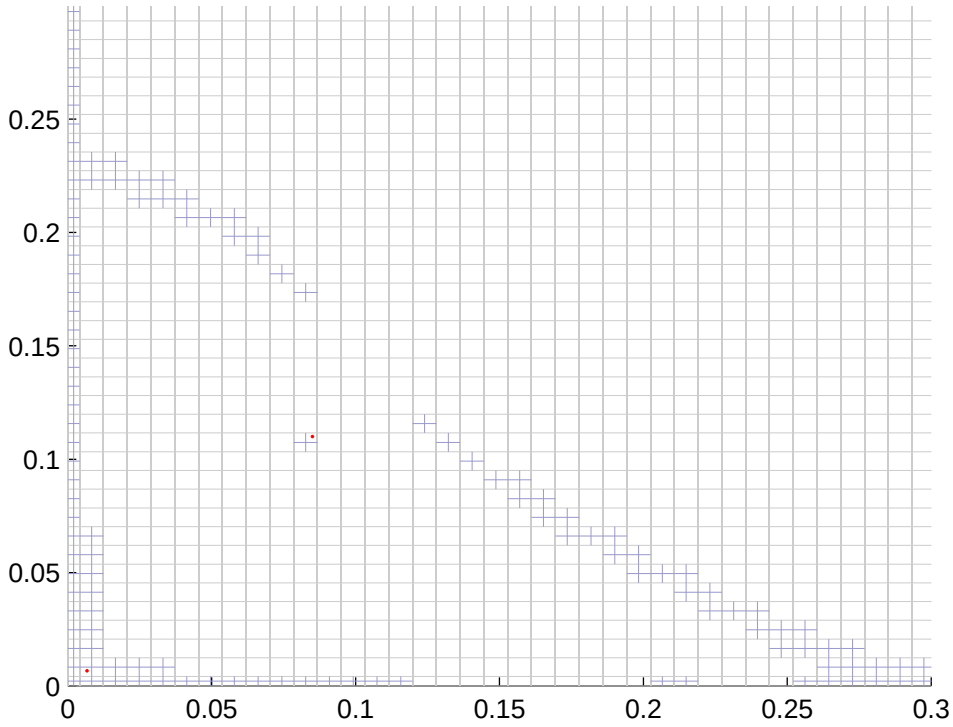

Fig. 13 Sub plot of bottom left corn of refined mesh for Re = 2500.

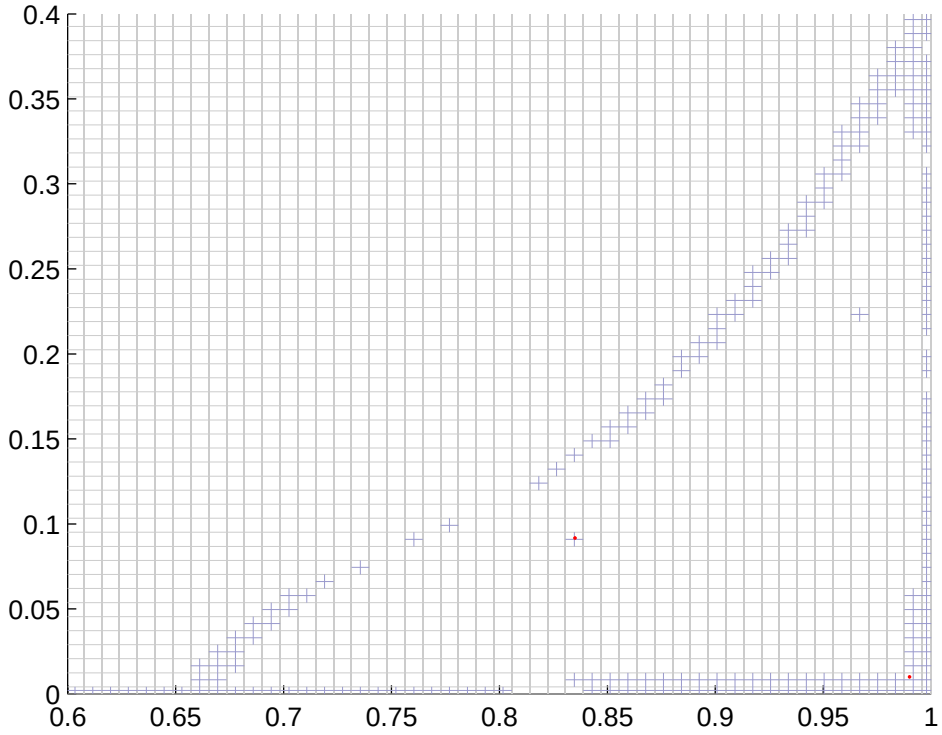

Fig. 14 Sub plot of bottom right corn of refined mesh for Re = 2500.

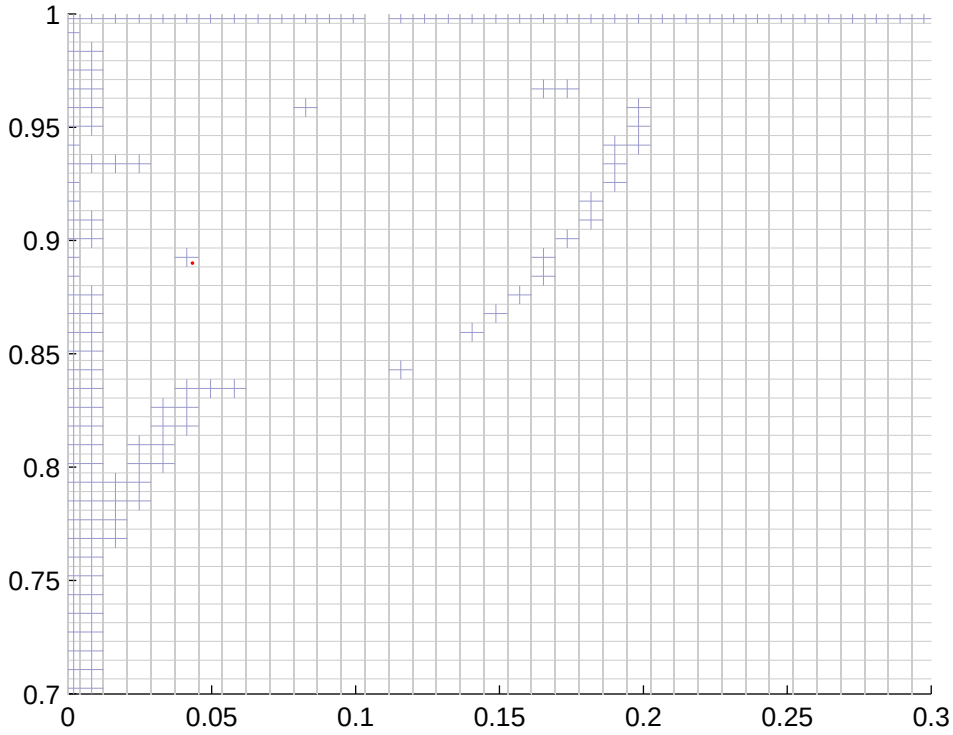

Fig. 15 Sub plot of top left corn of refined mesh for Re = 2500.